Regenerative Therapy 25 (2024) 49–60

Contents lists available at ScienceDirect

Regenerative Therapy

journal homepage: http://www.elsevier.com/locate/reth

Original Article

Development of triple-functionalized calcium phosphate nanoparticles as an advanced drug delivery system for bone tissue repair

Taichi Tenkumo [a, *], Benedikt Kruse [b], Kathrin Kostka [b], Viktoriya Sokolova [b], Toru Ogawa [a], Nobuhiro Yoda [a], Oleg Prymak [b], Osamu Suzuki [c], Keiichi Sasaki [a], Matthias Epple [b, **]

[a] Division of Advanced Prosthetic Dentistry, Tohoku University Graduate School of Dentistry, 4-1 Seiryo-machi, Aoba-ku, Sendai 980-8575, Japan
[b] Inorganic Chemistry and Center for Nanointegration Duisburg-Essen (CENIDE), University of Duisburg-Essen, Universitaetsstr. 5-7, D-45117 Essen, Germany
[c] Division of Craniofacial Function Engineering, Tohoku University Graduate School of Dentistry, 4-1 Seiryo-machi, Aoba-ku, Sendai 980-8575, Japan

ARTICLE INFO

Article history:
Received 7 September 2023
Received in revised form
8 November 2023
Accepted 16 November 2023

Keywords:
BMP-7
VEGF-A
TNF-α
Gene silencing
Gene transfection
Bone regeneration

ABSTRACT

Introduction: During tissue repair or regeneration, several bioactive molecules are released and interact with each other and act as complex additives or inhibitors for tissue reconstruction. In this study, the bone-healing effects of the combination treatment with tumor necrosis factor-α (TNF-α) inhibition, vascular endothelial growth factor A (VEGF-A) and bone morphogenetic protein-7 (BMP-7) release by gene silencing, and gene transfection with calcium phosphate nanoparticles (CaP) in the rat femoral head was histologically, morphologically, and biochemically evaluated.
Methods: A triple-functionalized paste of CaP carrying plasmid DNA encoding for BMP-7 and for VEGF), and siRNA against TNF-α was developed and denoted as CaP3mix. To compare the effects of 3mixCaP, CaP with plasmid DNA encoding BMP-7, VEGF, or siRNA encoding TNF-α was prepared and denoted as CaP/PEI/pBMP-7/SiO_2, CaP/PEI/pVEGF/SiO_2, or CaP/PEI/siRNA-TNF-α/SiO_2, respectively. The bone healing in bone defects in the rat femoral head was investigated after 10 and 21 days of implantation.
Results: The levels of bone formation-related markers OCN, Runx2, and SP7 increased at the protein and gene levels in 3mixCaP after 10 days, and 3mixCaP significantly accelerated bone healing compared with the other treatments after 21 days of implantation.
Conclusion: The triple-functionalized CaP paste loading plasmid DNA encoding BMP-7 and VEGF and siRNA encoding TNF-α is a promising bioactive material for bone tissue repair.

1. Introduction

During tissue repair or regeneration, several bioactive molecules are released in a time-dependent manner, and they interact with each other and act as complex additives or inhibitors for tissue reconstruction [1,2]. Many studies have investigated the effect of a single agent or combination of growth factors or inflammatory cytokines in vitro and in vivo [3–5]. Among these bioactive molecules, bone morphogenetic protein-7 (BMP-7) is one of the bone formation growth factors, and it shows strong bone formation activity in vivo and even in clinical applications [6,7]. Furthermore, BMP-7 directly stimulates osteoblasts and enhances osteoblast

Abbreviations: CaP, calcium phosphate; BMP-7, bone morphogenetic protein-7; VEGF-A, Vascular endothelial growth factor A; TNF-α, tumor necrosis factor-α; PEI, branched polyethyleneimine; ALP, alkaline phosphatase; ELISA, enzyme-linked immunosorbent assay; FBS, fetal bovine serum; OCN, Osteocalcin.

* Corresponding author.
** Corresponding author. Inorganic Chemistry, University of Duisburg-Essen, Universitaetsstr. 5-7, D-45117 Essen, Germany.
E-mail addresses: taichi.tenkumo.a3@tohoku.ac.jp (T. Tenkumo), matthias.epple@uni-due.de (M. Epple).

Peer review under responsibility of the Japanese Society for Regenerative Medicine.

https://doi.org/10.1016/j.reth.2023.11.010

differentiation [7,8]; thus, it is used to enhance the bioactivity of bone grafts [9].

In contrast, vascularization is essential for tissue reconstruction. Blood vessels supply nutrients, gas changes, bioactive molecules such as growth factors or cytokines, and cells [10,11]. Vascular endothelial growth factor (VEGF) is an angiogenic growth factor that has been shown to be effective in bone tissue engineering models [3–5,10,11]. Furthermore, previous studies have shown that the combination of VEGF and BMPs, such as BMP2, BMP4, and BMP-7, can enhance successful bone formation through BMP/VEGF-regulated coupling between osteogenesis and angiogenesis [12,13].

In wound healing, tissue repair follows the inflammation process [1]; however, adequately inhibiting inflammation during bone tissue repair enhances bone formation [14–16]. Ratanavaraporn et al. demonstrated that adequate inhibition of TNF-α enhance bone regeneration induced by BMP-2 [17]. We have also previously demonstrated that the inhibition of TNF-α by gene silencing removes the suppression of ALP activity in periodontal tissue-derived cells stimulated by inflammation [18].

BMP-7, VEGF, and TNF-α are associated with bone formation in different ways; therefore, we hypothesize that bone formation-associated cells recruited by vascularization are stimulated by growth factors and effectively form bone tissue under the adequate inhibition of inflammation. To enhance this process, we focused on gene transfection and gene silencing techniques. Gene transfection vectors are mainly classified as viral and nonviral vectors, and numerous vectors or gene carriers have been developed, improved, and used [19,20]. In our study, calcium phosphate was used as gene carrier. Although its transfection efficiency is lower than that of viral transfection or liposomes and similar systems, calcium phosphate has the advantage that it is the inorganic component of bone tissue and therefore has a high biocompatibility and biodegradability. Consequently, it is a highly suitable material for bone regeneration [21]. We have previously developed gene carriers based on calcium phosphate nanoparticles (CaP) and demonstrated low cell cytotoxicity, improved gene transfection efficiency, and gene silencing in vitro and in vivo [18,22–31].

In this study, the bone-healing effects of the combination treatment with TNF-α inhibition by gene silencing, VEGF-A and BMP-7 release by gene transfection with CaP nanoparticles in the rat femoral head was histologically, morphologically, and biochemically evaluated.

2. Materials and methods

2.1. Chemicals

Diammonium hydrogen phosphate ($(NH_4)_2HPO_4$; ≥99 %), branched polyethyleneimine (PEI, MW: 25 kDa), tetraethyl orthosilicate (TEOS, ≥99 %), ammonia solution (28 wt% NH_3 in water), sodium hydroxide (≥98 %), and D-(+)-trehalose dihydrate were obtained from Sigma-Aldrich (St. Louis, MO, USA). Calcium lactate pentahydrate ($CaC_6H_{10}O_6 \cdot 5H_2O$; ≥98 %) and carboxymethyl cellulose sodium salt (≥99.5 %, powdered) were obtained from Carl Roth (Karlsruhe, Germany). Ethanol (99.8 %) was purchased from ThermoFisher Scientific (Darmstadt, Germany). The plasmids for VEGF (VEGF-A, human untagged clone, Vector: pCMV6-XL5, Vector size: 4.7 kb, promoter: CMV, ACCN: NM_001025366) and BMP-7 (product name: BMP7, human untagged clone, Vector: pCMV6-XL4, Vector size: 4.7 kb, promoter: CMV, ACCN: NM_001719) were purchased from OriGene (Herford, Germany). siRNA-TNF-a (small interfering RNA against tumor necrosis factor-α, 5'-GCCGAUGGGUUGUACCUUG-3') was purchased from Dharmacon (Lafayette, CO, USA). Ultrapure water (Purelab Ultra Instrument, ELGA) with a specific resistivity of 18.2 MΩ was used for all syntheses. An endotoxin-free plasmid DNA purification kit NucleoBond® PC 10000 EF was purchased form Macherey-Nagel (Düren, Germany).

Four types of CaP-NPs were prepared: CaP-NPs coated with carboxymethyl cellulose (CMC) as a matrix, CaP-NPs carrying DNA plasmid encoding for VEGF, CaP-NPs carrying DNA plasmid encoding for BMP-7, and CaP-NPs carrying siRNA against TNF-α, respectively (CaP/CMC, CaP/VEGF, CaP/BMP-7, and CaP/siRNA-TNF-α).

2.1.1. Synthesis of plasmid

The plasmids pVEGF and pBMP-7 were amplified by naturally competent *E. coli* bacteria. Isolation and purification were performed according to the manufacturer's protocol with a Giga kit (AX 10000, Macherey-Nagel).

2.1.2. Synthesis of CaP nanoparticles

CaP nanoparticles were prepared according to our previous reports [18,21,30]. For the synthesis of CaP nanoparticles, aqueous solutions of calcium lactate (6.25 mM) and diammonium hydrogen phosphate (3.74 mM) were adjusted to pH 10 with NaOH (0.1 M). Additionally, an aqueous solution of PEI (2 g L^{-1}) was prepared. The three solutions were pumped simultaneously into a round bottom flask containing 10 mL ultrapure water during 30 s with peristaltic pumps at 5 mL min^{-1} for the calcium lactate and diammonium hydrogen phosphate solutions, respectively, and 7 mL min^{-1} for the PEI solution. After reacting for 20 min under stirring, 5.40 mL of the CaP/PEI nanoparticle dispersion was taken, and 600 μL of either plasmid (pVEGF or pBMP-7; 1 mg mL^{-1}) or 996 μL of siRNA (0.6 mg mL^{-1}), respectively, was added under RNase-free conditions. The dispersion was stirred for 30 min. Then, a protective silica shell was added to the particles to prevent enzymatic degradation of the nucleic acids. Next, 6 mL of dispersion was added to a mixture of 24 mL of ethanol, 30 μL of TEOS, and 60 μL of ammonia solution (7.8 wt%). The reaction was stirred for 18 h at room temperature. To isolate the nanoparticles, they were centrifuged for 60 min at 4000 rpm. The supernatant was analyzed by UV microvolume spectroscopy (DS-11 FX+, DeNovix) to determine the loading on the nanoparticles. The sedimented particles were redispersed by ultrasonication in 6 mL of ultrapure water for endotoxin analysis. With an Endosafe Nexgen-PTS spectrometer (Charles River, Boston, MA, USA), the endotoxin concentration in all samples was determined to be below 0.0133 EU mL^{-1}. Thus, the samples were considered as endotoxin-free.

Next, 1.5 mL of each nanoparticle sample carrying nucleic acids (pVEGF, pBMP-7, and siRNA) was taken and mixed to obtain a total volume of 4.5 mL for each group; it is denoted as 3mixCaP hereafter. All nanoparticles were aliquoted to 300 μL per tube, each containing 20 μg of pDNA or siRNA; they were freeze-dried with D-(+)-trehalose dihydrate as a cryoprotectant (20 mg per 1 mL of dispersion) for 72 h for storage and shipping (lyophilization; Alpha 2-4 LSC instrument, Martin Christ). The 3mixCaP sample contained a total combined dose of 60 μg of pDNA and siRNA, i.e. 20 μg of each nucleic acid.

2.1.3. Synthesis of the CaP paste matrix

For the preparation of the CaP paste matrix, calcium lactate (6.25 mM) and diammonium hydrogen phosphate (3.74 mM) were adjusted to pH 10 with NaOH (0.1 M). Additionally, an aqueous solution of carboxymethyl cellulose (CMC, 2 g L^{-1}) was prepared. The three solutions were pumped simultaneously into a round bottom flask containing 100 mL of ultrapure water over 5 min with peristaltic pumps at 7.5 mL min^{-1} for the calcium lactate and diammonium hydrogen phosphate solutions, respectively, and 2.5 mL min^{-1} for the CMC solution. After reacting for 10 min under

stirring, the dispersion was centrifuged at 4000 g for 30 min. The precipitated nanoparticles were redispersed in ultrapure water. The sample was shock-frozen in liquid nitrogen and freeze-dried. After freeze-drying, the yield of CMC-functionalized CaP nanoparticles was ≈1.2 g as solid.

To prepare a bioactive paste, 20 μg of the desired freeze-dried plasmid or siRNA loaded onto the particle surface was mixed with 16.68 mg of the CaP/CMC matrix, as shown in Table 1. In the case of 3mixCaP, 20 μg of each bioactive component was used. To obtain the bioactive CMC paste matrix, 64 μL of water was added to each group.

2.1.4. Physicochemical characterization

The calcium concentration was measured by atomic absorption spectroscopy (AAS) with an Electron M-Series spectrometer (ThermoScientific). Dynamic light scattering (DLS) and zeta potential determination were carried out with a Zetasizer Ultra (Malvern Panalytical) in a disposable cuvette (DTS1070). Scanning electron microscopy (SEM) was performed with an ESEM Quanta 400 FEG instrument (FEI). Thermogravimetric analysis (TGA) was conducted with a STA 449 F3 Jupiter instrument (Netzsch). Microvolume UV–Vis absorbance spectra were recorded with a Genesis 50 instrument (ThermoScientific). Microplate absorbance was measured with a SpectraMax 190 instrument (Molecular Device). Freeze-drying (lyophilization) was performed with a Christ Alpha 2-4 LSC instrument (Martin Christ).

2.2. Animal experiments

2.2.1. Application of CMC-functionalized CaPs

Thirty eight male Wistar rats (age: 6 weeks; weight: 180–200 g) were used in this experiment. All animals were used in this experiment in accordance with the Guide for the Care and Use of Laboratory Animals of Tohoku University, Japan. Prior to the experiments, the experimental protocols were reviewed and approved by the Institutional Animal Experiment Committee of Tohoku University (No. 2020shidou-026). The rats were anesthetized by the intraperitoneal injection of medetomidine (Domitor®; 0.375 mg kg^{-1} body weight; Nippon Zenyaku Kogyo, Tokyo, Japan), midazolam (Sandoz; 2 mg kg^{-1} body weight; Sandoz, Tokyo, Japan), and butorphanol tartrate (Vetorphale®, 2.5 mg kg^{-1} body weight; Meiji Seika Co., Tokyo, Japan). After general anesthesia, local anesthesia with lidocaine containing epinephrine (1:80,000) was administered around the thigh muscle. The hair of each rat was shaved, the flap was reflected, muscle and tendon were shaved, and the femoral head was exposed. The bone defect was prepared using a dental implant drill (diameter: 3.1 mm; Fig. 1a and c) at 3000 rpm with sterile saline irrigation using a dental electric motor system (Implant Motor IM-III, GC, Japan). The prepared bone defect volume was 21.36 mm^3 (Fig. 1b). The prepared CMC-functionalized CaP paste (16.38 mg) was tightly inserted into the bone defect (Fig. 1d). The muscle, tendon, and skin flap were independently tightly sutured with nonabsorbable suture (7-0NYLON, Mani Inc., Tochigi, Japan) to prevent infection and loss of biomaterial, respectively. The rats were sacrificed by an overdose of Isoflurane (Fujifilm Wako chemicals, Tokyo, Japan) on days 10 and 21 after surgery. The femoral bone head including the surrounding tissue was extracted and immediately immersed in phosphate-buffered saline (PBS). Seventy-five bone defects were prepared in total. Each rat was treated with a split-mouth design; this implies that different samples were implanted in both sides of the femoral head. One rat obtained CaP/PEI/pBMP-7/SiO_2 in the left femoral head and CaP/PEI/pVEGF/SiO_2 in the right femoral head, whereas the other rat obtained CaP/PEI/pVEGF/SiO_2 in the left femoral head and CaP3mix in the right femoral head. The sample number in each group was 15 bone defects in total. The transverse plane of the bone defect is shown in Fig. 1b.

2.2.2. Gene analysis

All plastic pipette tips and tubes were soaked for 1 min in RNase Quiet (Nacalai Tesque, Japan) to remove RNAses. After discarding the solution, the tips and tubes were rinsed thoroughly two times with ultrapure water, dried, and finally autoclaved for 20 min at 121 °C. The femoral head of the extracted tissue was cut 10 days after the surgery for gene analysis. The tissue was washed with PBS and immersed in 1 mL of Sepasol RNA I Super G® (Nacalai Tesque Inc., Kyoto, Japan) for gene analysis. Tissues were crushed and homogenized for 10 s using an ultrasonicator (UR-20P, 21 kHz; Tomy Co. Ltd., Tokyo, Japan). Total RNA was isolated from the supernatant according to the manufacturer's instructions, and the total volume of extracted mRNA was measured by UV microvolume spectroscopy (Nanodrop2000; Thermo Scientific, Tokyo, Japan). Furthermore, DNase treatment was performed using DNase buffer (Takara, Japan), RNase inhibitor (Takara, Japan), and DNase I (Takara, Japan) as per the manufacturer's instructions. The total volume of RNA after the DNase treatment was measured again, resuspended in TE buffer (Nacalai, Japan), and stored at −20 °C until gene analysis was performed. After measuring the concentration of the obtained RNA, cDNA was synthesized using the iScript Advanced cDNA Synthesis Kit for RT-qPCR® (Bio-Rad Laboratories, Osaka, Japan). Real-time polymerase chain reaction (PCR) was performed using CFX96 (Bio-Rad, Osaka, Japan) with 10 ng of cDNA in a 20 μL of a mixture containing 10 μL of SsoAdvanced Universal SYBR Green® system (Bio Rad Laboratories, Osaka, Japan), 7 μL of DNase-free water, and 1 μL of targeted primer. The following primers were used: OCN (PrimePCR SYBR Assay, Unique Assay ID:qRnoCED0007311, Desalt 200R Wet-Validated, Predesign Bglap, rat, Bio-Rad, Japan), GAPDH (PrimePCR SYBR Assay, Unique Assay ID:qRnoCID0057018, Desalt 200R Wet-Validated, Predesign GADPH, rat, Bio-Rad, Japan), Runx2 (PrimePCR SYBR Assay, Unique Assay ID:qRnoCED0009315, Desalt 200R Wet-Validated, Predesign Runx2, rat, Bio-Rad, Japan), and SP7 (PrimePCR SYBR Assay, Unique Assay ID: qRnoCED0008486, Desalt 200R Wet-Validated, Predesign SP7, rat, Bio-Rad, Japan). For reliability, no template control (primer-only and DNase-free water) was used. The reaction mixture was incubated for polymerase activation and DNA denaturation at 98 °C for 30 s. For amplification,

Table 1
Dosage of plasmid-DNA or siRNA in each CMC-functionalized CaP group.

	Dose/defect			
group	pBMP-7/μg	pVEGF/μg	siRNA (TNF-α)/μg	CaP nanoparticles/mg
CaP/CMC				16.68
CaP/PEI/BMP-7/SiO_2	20.0			16.68
CaP/PEI/VEGF/SiO_2		20.0		16.68
CaP/PEI/siRNA-TNF-α/SiO_2			20.0	16.68
3MixCaP	20.0	20.0	20.0	16.68

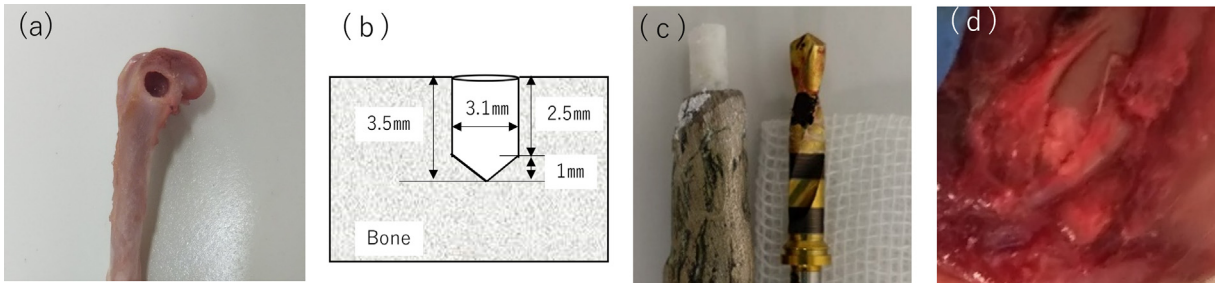

Fig. 1. (a) Bone defect in the rat femoral head. (b) Cross section of prepared bone defect. The bone defect volume was 21.4 mm^3. (c) Left: A delivery tool for the regulated volume of CaP paste. Right: A dental implant drill with black line markers to prepare regulated bone defects. (d) CaP paste inside the bone defect.

the reaction mixture was subjected to 40 cycles of denaturation at 95 °C for 10 s and annealing/extension at 60 °C for 30 s. The reference gene, glyceraldehyde 3-phosphate dehydrogenase (GAPDH), was determined by comparison with β-actin using the Bestkeeper© software. The mRNA expression level of each targeted gene was determined using GAPDH as the normalization control and the ΔΔ CT method. The experiment was independently performed on five samples from each experimental group, and three measurements were performed independently. The sample number in each group was five, as there were five bone defects.

2.2.3. ELISA

To measure the levels of TNF-α, BMP-7, VEGF, BMP-2, CD31, and ALP, the femoral head of the extracted tissue after 10 days of surgery was cut and dissolved in 600 μL of a RIPA Lysis Buffer® solution (Santa Cruz Biotechnology, Dallas, TX, USA), ultrasonically homogenized for 10 s, and centrifuged at 16,099×*g* for 15 min at 4 °C. TNF-α, BMP-7, VEGF, BMP-2, CD31, and ALP in the supernatants were quantified by ELISA using Rat TNF-α ELISA (Abcam, Cambridge, England), Rat BMP7 ELISA (Mybiosource, San Diego, USA), Rat VEGF ELISA (proteintech, Tokyo, Japan), BMP-2 Quantikine ELISA (R&D Systems, Minneapolis, USA), Rat Pecam1/CD31 ELISA Kit (Assay Genie, Dublin, Ireland), and LabAssay ALP (Wako Pure Chemical Industries Ltd., Osaka, Japan) kits, respectively. The total protein concentrations of the cell lysates were determined using the bicinchoninic acid (BCA) protein assay kit (Takara, Shiga, Japan). The absorbance of the reaction mixture was measured using a microplate reader (SpectraMax 190; Molecular Devices, San Jose, USA) according to the manufacturer's instructions. The measured value of each protein were normalized by the total protein volume. The supernatants were stored at 20 °C until the measurements were performed. The sample number in each group was five, as there were five bone defects.

2.2.4. Western blotting

To detect the protein levels of OCN, Runx2, and SP7, tissue lysates after 10 days of surgery prepared using RIPA lysis buffer in Section 2.3.3 were diluted by Laemmli sample buffer (#1610737; Bio-Rad, Hercules, USA) and used for Western blotting. Equal amounts of protein were resolved using Mini-PROTEAN TGX gel (2 % SDS-PAGE, 62.5 mM TriHCl (pH 6.8), 25 % glycerol; Bio-Rad, Hercules, USA) at 200 V and 400 mA for 30 min. Then, the proteins were transferred to a nitrocellulose membrane (Trans-Blot Turbo Mini 0.2 μm PVDF transfer packs, Bio-Rad, Hercules, USA) using a Trans-Blot Turbo transfer system (Bio-Rad, Hercules, USA) at 1.3 A and 25 V for 7 min. After washing and blocking using Blocking One (Nacalai Tesque, Kyoto, Japan) for 30 min, the membrane was washed and immersed in immunoreaction buffer containing anti-OCN (1:1000, Monoclonal antibody to rat osteocalcin (Clone6-7H), Takara bio, Shiga, Japan), anti-Runx2 (1:1000, Anti RUNX2 (ab76956); Abcam, Cambridge, England), anti-SP7 (1:1000, Anti-Sp7/Osterix antibody (EPR21034); Abcam, Cambridge, England), or anti-beta actin (1:1000, anti-β-actin antibody (ab8227); Abcam, Cambridge, England). Then, the membrane was incubated while shaking overnight at 4 °C. After washing, the membrane was immersed in Bullet ImmunoReaction Buffer containing a secondary antibody (horseradish peroxidase (HRP)-conjugated Affinipure goat anti-rabbit IgG (H + L), 1:5000). The immunoreactivity was visualized using the ECL system (Chemi-Lumi One Super, Nacalai Tesque, Kyoto, Japan). Western blotting was performed, and the intensity of each band was quantified using a chemiluminescence imaging system (FUSION, Vilber Bio Imaging, Osaka, Japan). The obtained OCN, RUNX2, and SP-7 values were normalized by the obtained value of anti-beta actin. The sample number in each group was five, as there were five bone defects.

2.2.5. Microcomputed tomography (μCT)

The extracted samples after 21 days of surgery were scanned using microcomputed tomography (ScanXmate-E090; 60 kV; 80 μA; Comscan Tecno Co. Ltd., Kanagawa, Japan) on the same day. Bone defect volumes were measured at 238.75 mg/cm^3 of the threshold using Image J software (National Institutes of Health, Bethesda, MS, USA). A three-dimensional (3D) image of the extracted femoral head was constructed using a 3D structural analysis software (RATOC TRI/3D-BON; Ratoc System Engineering Co. Ltd., Tokyo, Japan).

2.2.6. Histological observation

After scanning, the extracted tissue was fixed in 4 % paraformaldehyde-PBS for 1 day and then washed with water for 2 days for histological observation. The extracted tissue was decalcified with 17.7 % EDTA (OSTEOSOFT®, Merck Millipore, Tokyo, Japan) for 14 days and washed by water and finally embedded in paraffin. Tissue sections with a thickness of 6 μm were prepared using a microtome and then stained with hematoxylin and eosin. The sliced sections were stained with an anti-rat TNF-α monoclonal antibody (1:1000 in PBS; TaKaRa Bio, Shiga, Japan), anti-OCN (1:2000, monoclonal antibody to rat osteocalcin (Clone6-7H), Takara bio, Shiga, Japan), anti-Runx2 (1:50, Anti RUNX2 (ab76956); Abcam, Cambridge, England), and anti-SP7 (1:500, Anti-Sp7/Osterix antibody (EPR21034); Abcam, Cambridge, England). Briefly, tissue sections were incubated overnight with an anti-TNF-α antibody at 4 °C. After extensive washing of cells with a PBS solution, the bound antibodies were detected using the Histofin Simple Stain MAX PO reagent (Nichirei Biosciences, Tokyo, Japan) and diaminobenzidine tetrahydrochloride as the substrate. The stained sections were observed under a light microscope.

2.3. Statistical analysis

All data are presented as mean ± standard deviation (SD). The normal distribution of the data was verified using the Shapiro–Wilk test. All the data were assumed to be normally distributed. Statistical differences between groups were assessed by analysis of variance followed by the post-hoc Tukey–Kramer HSD multiple comparison test. Statistical analyses were performed using SPSS 22.0 (IBM Japan, Tokyo, Japan). Differences were considered statistically significant at $p < 0.05$.

3. Results and discussion

The aim of this study was to evaluate the bone-healing effects of TNF-α inhibition by gene silencing, and VEGF/BMP-7 formation via gene transfection with CaP nanoparticles loading DNA encoding for BMP7 and VEGF, and siRNA against TNF-α in CaP paste in the rat femoral head. First, the dispersed nanoparticles were analyzed. The nanoparticle properties are summarized in Table 2. Dynamic light scattering (DLS) revealed that the hydrodynamic diameter of the dispersed nanoparticles ranged from 93 to 206 nm (Fig. 2), with a polydispersity index (PDI) of approximately 0.34 (Table 2). Due to cationic polymeric stabilization with PEI, the zeta potential was approximately +18 mV. SEM revealed an approximately spherical morphology with a solid core diameter of 55–83 nm (Fig. 3). Fig. 4 shows the TGA results: Approximately 17.4 wt% CMC and 66.2 wt% CaP were found, with the remaining 9.3 wt% being water.

These characterization steps and results were the same as those reported for the CaP nanoparticles in our previous studies [18,22,31]. Thus, tentatively, the CaP nanoparticles prepared in this study were considered to have the same gene transfection and gene silencing efficiency as those prepared in our previous studies. There, gene transfection or gene silencing using CaP nanoparticles in HeLa cells, MG-63, human mesenchymal stem cells, monocyte macrophages, rat bone marrow-derived cells, and rat gingival-derived cells were reported [18,22,29,30].

Fig. 5 shows the result of the release of the target proteins in the femoral head after 10 days of surgery. The amount of TNF-α released after treatment with CaP/PEI/siRNA-TNF-α/SiO_2 was statistically the lowest among all groups, and the amount of TNF-α released in 3mixCaP was significantly lower than those of CaP/CMC, CaP/PEI/pVEGF/SiO_2, and CaP/PEI/pBMP-7/SiO_2 (Fig. 5A). The amount of BMP-7 released in CaP/PEI/pBMP-7/SiO_2 was statistically the highest among all groups, and the amount of BMP-7 released in 3mixCaP was significantly higher than those of CaP/CMC, CaP/PEI/pVEGF/SiO_2, and CaP/PEI/siRNA-TNF-α/SiO_2 (Fig. 5B). The amount of VEGF released in CaP/PEI/pVEGF/SiO_2 was the highest in all groups and that of 3MixCaP was significantly higher than that in CaP/CMC and CaP/PEI/pBMP-7/SiO_2 (Fig. 5C). This result indicates that both gene silencing and gene transfection were successful in the femoral head during 10 days after CaP implantation.

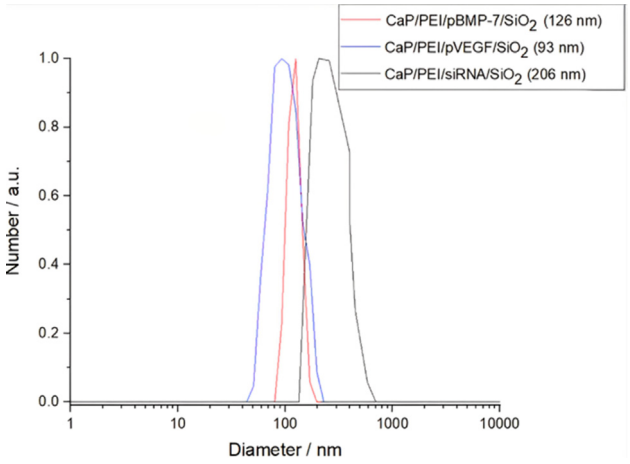

Fig. 2. Representative dynamic light scattering (DLS) measurements of the four nanoparticle samples, together with the particle size distribution by number.

However, the combined gene silencing effect or gene transfection effect in 3mixCaP was smaller than that in CAP/CMC loaded with a single-plasmid DNA or siRNA only. This suggests that the limited number of migrating cells might limit the gene transfection or silencing effects. The number of transgenic cells with plasmid DNA-coded BMP-7 in 3mixCaP might be fewer than that with CaP/PEI/pBMP-7/SiO_2, and other cells in the application of 3mixCaP might be transgenic with plasmid DNA-coded VEGF or siRNA-coded TNF-α. We previously demonstrated that the total amount of the released proteins resulting from gene transfection was approximately the same in the case that several kinds of plasmid-DNA are applied at same time [27].

Next, the bone formation activity at 10 days after surgery was biochemically investigated. The amounts of BMP-2 released in 3mixCaP was the highest among all groups, and the amounts of BMP-2 released in CaP/PEI/pBMP-7/SiO_2 and CaP/PEI/siRNA-TNF-α/SiO_2 were significantly higher than those of CaP/CMC and CaP/PEI/pVEGF/SiO_2 (Fig. 5E). High concentration of BMP-2 released in local area indicates high bone formation activity. The ALP activities of 3mixCaP, CaP/PEI/pBMP-7/SiO_2, and CaP/PEI/siRNA-TNF-α/SiO_2 were significantly higher than those of CaP/CMC and CaP/PEI/pVEGF/SiO_2 (Fig. 5F).

Fig. 6 shows the results of the expression level of the bone-related proteins in the femoral head 10 days after CaP application by Western blotting. Runx2 and SP-7 are absolute requirement for

Table 2
Properties of prepared CaP nanoparticles. PDI: polydispersity index, measured with DLS.

Sample (dispersion)	CaP/PEI/siRNA/SiO_2	CaP/PEI/pVEGF/SiO_2	CaP/PEI/pBMP-7/SiO_2	CaP/CMC
Solid core particle diameter by SEM/nm	55 ± 7	83 ± 12	59 ± 9	71 ± 10
V (one nanoparticle; only CaP)/m^3	$8.71 \cdot 10^{-23}$	$2.99 \cdot 10^{-22}$	$1.07 \cdot 10^{-22}$	$8.71 \cdot 10^{-23}$
m (one nanoparticle; only CaP)/kg	$2.73 \cdot 10^{-19}$	$9.40 \cdot 10^{-19}$	$3.37 \cdot 10^{-19}$	$2.73 \cdot 10^{-19}$
$w(Ca^{2+})$ in the dispersion by AAS/kg m^{-3}	0.098	0.073	0.076	25 wt%
$w(Ca_5(PO_4)_3OH)$ in the dispersion/kg m^{-3}	0.246	0.183	0.191	–
N(nanoparticles) in the dispersion/m^{-3}	$8.99 \cdot 10^{+17}$	$1.95 \cdot 10^{+17}$	$5.64 \cdot 10^{+17}$	–
Hydrodynamic particle diameter by DLS/nm	206	93	126	–
Polydispersity index (PDI) by DLS	0.36	0.32	0.35	–
Zeta potential by DLS/mV	+16	+20	+17	–
N(pDNA)/m^{-3}	$2.59 \cdot 10^{+22}$	$2.02 \cdot 10^{+22}$	$2.15 \cdot 10^{+22}$	–
m(pDNA) per nanoparticle/kg	$6.46 \cdot 10^{-19}$	$2.93 \cdot 10^{-18}$	$9.92 \cdot 10^{-19}$	–
N(pDNA) molecules per particle	$2.88 \cdot 10^{+4}$	$1.04 \cdot 10^{+5}$	$3.81 \cdot 10^{+4}$	–
Endotoxin/EU·mL^{-1}	< 0.01	0.0133	0.0126	<0.01

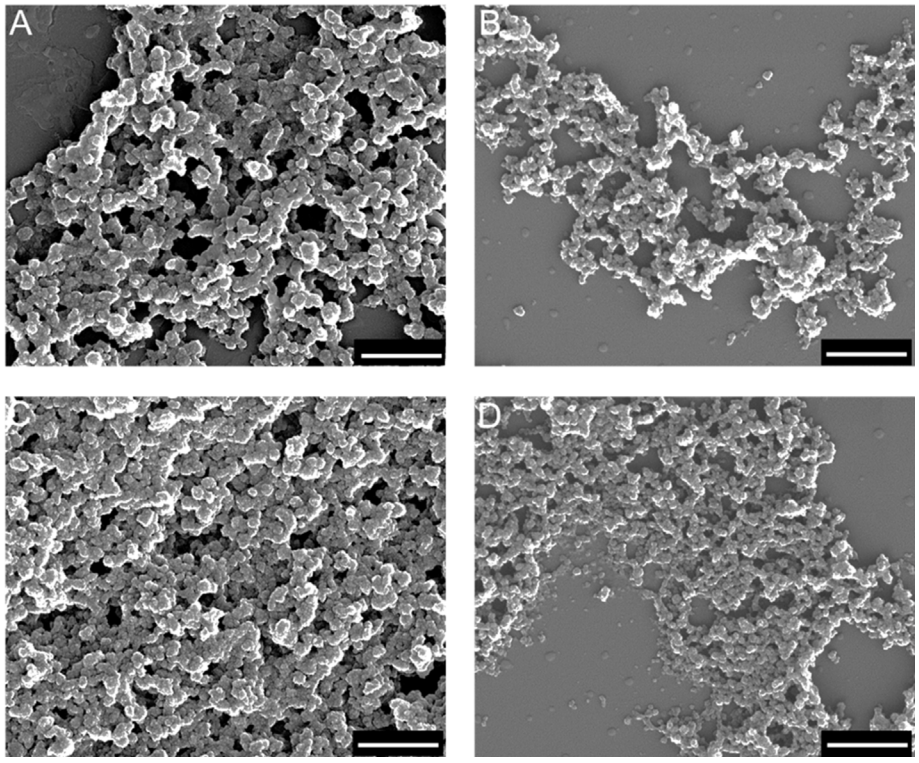

Fig. 3. Representative scanning electron microscopy (SEM) images of the four nanoparticle samples: (A) CaP/PEI/pVEGF-A/SiO_2, (B) CaP/PEI/pBMP-7/SiO_2, (C) CaP/PEI/siRNA-TNF-α/SiO_2, and (D) CaP/CMC paste matrix. Scale bars = 500 nm.

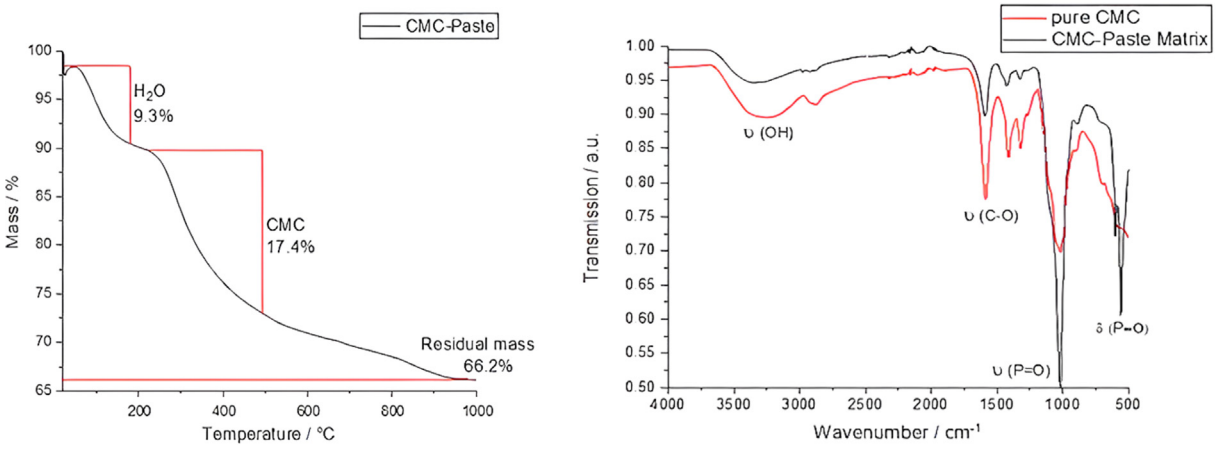

Fig. 4. Left: Representative results from thermogravimetric analysis (TGA) of the CaP/CMC pastes matrix. Right: Infrared spectra (IR) of the pure CMC powder (red) and CaP/CMC paste matrix (black).

osteoblast differentiation and positively influences the early stages of osteoblast differentiation. On the other hand, OCN is expressed in a later stage of osteoblast differentiation. Therefore, the proteins level of OCN, Runx2 and SP-7 were investigated. The OCN levels in 3mixCaP, CaP/PEI/pBMP-7/SiO_2, and CaP/PEI/siRNA-TNF-α/SiO_2 were significantly higher than those in CaP/CMC and CaP/PEI/pVEGF/SiO_2. The Runx2 levels in CaP/PEI/siRNA-TNF-α/SiO_2 and 3mixCaP were significantly higher than those in CaP/CMC, CaP/PEI/pBMP-7/SiO_2, and CaP/PEI/pVEGF/SiO_2. The SP-7 levels in 3mixCaP were significantly higher than those in CMC/CaP, CaP/PEI/pBMP-7/SiO_2, and CaP/PEI/pVEGF/SiO_2. Fig. 7 shows the gene expression 10 days after CaP application. The OCN, Runx2, and SP7 gene expression levels in 3mixCaP were significantly higher than those of CaP/CMC and CaP/PEI/pVEGF/SiO_2. The OCN and Runx2 gene expressions of CaP/PEI/siRNA-TNF-α/SiO_2 were significantly higher than those in CMC/CaP and CaP/PEI/pVEGF/SiO_2. From these results, the bone formation activity at the protein and gene expression levels was highest in 3MixCaP at 10 days after surgery and this supports the result of next morphological observation.

In terms of bone tissue regeneration, the remaining bone defect volume of 3mixCaP was the lowest among all groups, and the remaining bone defect volumes in CaP/PEI/siRNA-TNF-α/SiO_2 and CaP/PEI/pBMP-7/SiO_2 were significantly smaller than those in CaP/CMC and CaP/PEI/pVEGF/SiO_2 (Fig. 8a). The remaining CaP material

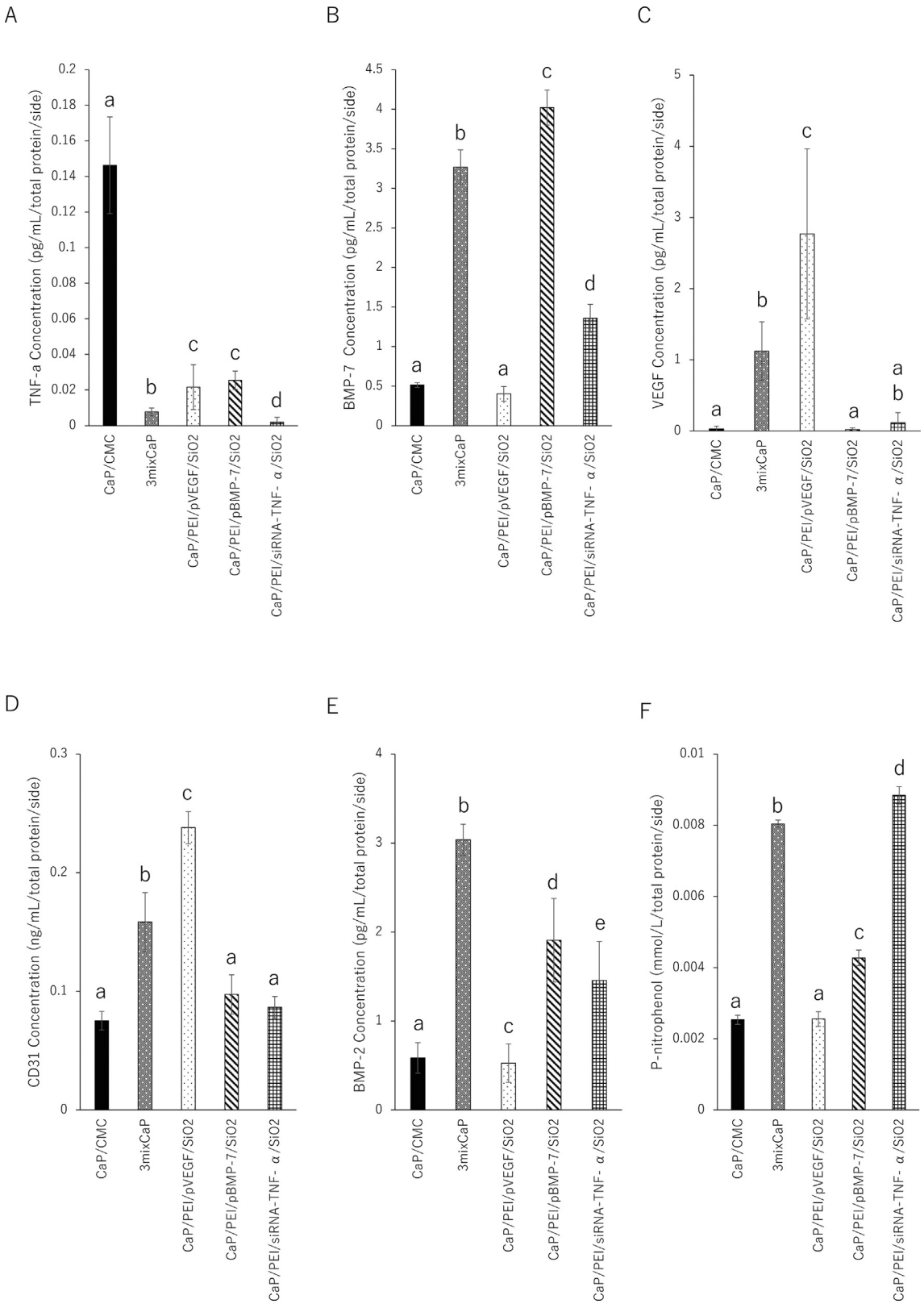

Fig. 5. Biochemical analyses by ELISA. Released volumes of (A) TNF-α, (B) BMP-7, (C) VEGF, (D) CD31, (E) BMP-2, and (F) ALP after 10 days of implantation in the femoral head. The number of samples in all groups was five. Significant differences ($p < 0.05$) between the groups at each time point are denoted by different superscript letters (i.e., bars with the same letter are not significantly different).

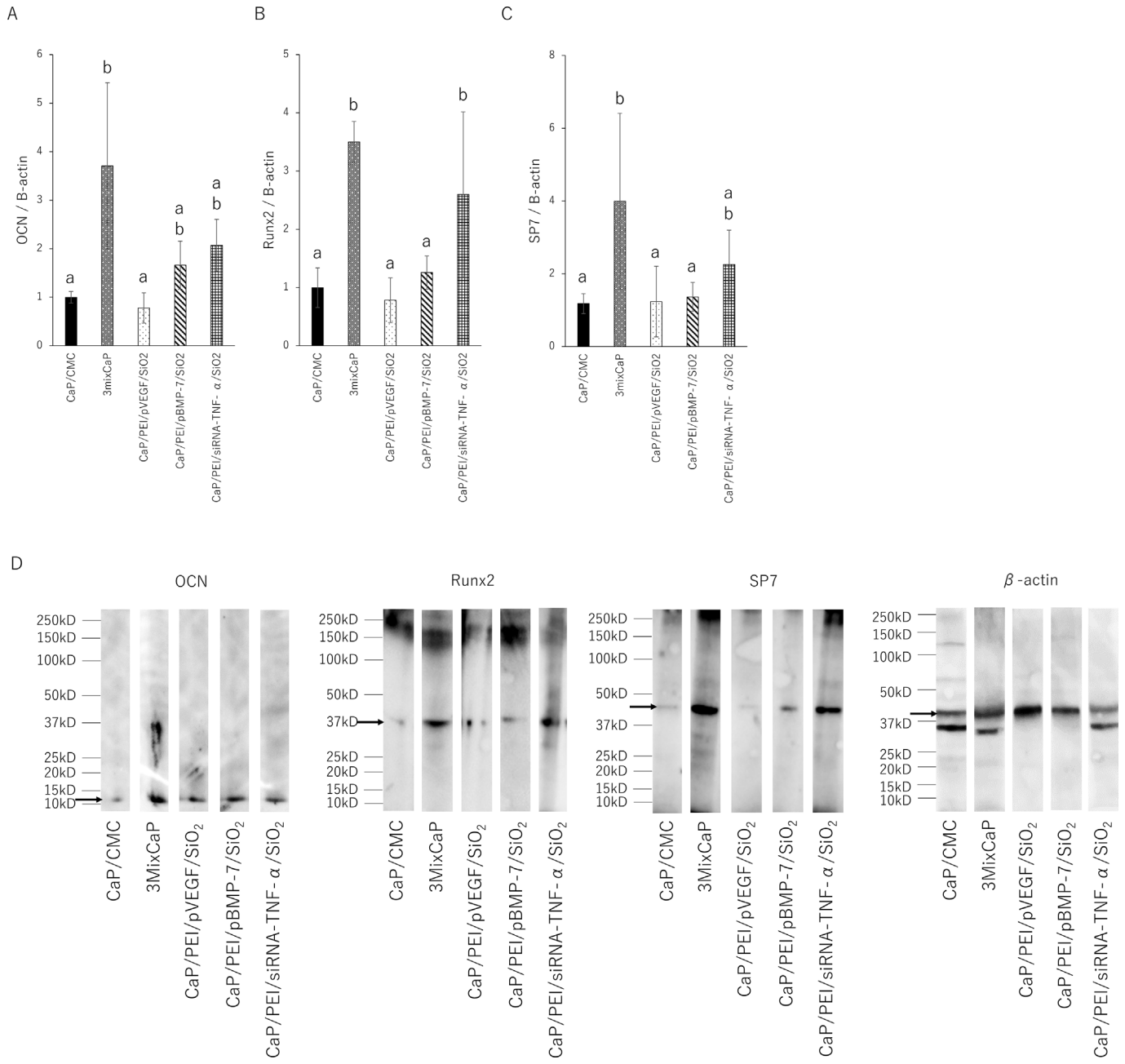

Fig. 6. Biochemical analyses by Western blot. Concentrations of (A) OCN, (B) Runx2, and (C) SP-7 (Osterix) after 10 days of implantation in the femoral head. The expression level of each targeted protein was calculated using β-actin as the normalization control. The number of samples in all groups was five. Significant differences ($p < 0.05$) between the groups at each time point are denoted by different superscript letters (i.e., bars with the same letter are not significantly different). (D) Representative images of OCN, Runx2, SP-7, or β-actin band on membrane.

was clearly observed in CaP/CMC and CaP/PEI/pVEGF/SiO_2 but not in 3mixCaP (Fig. 8b). Neither infection nor severe inflammation, necrosis, or drainage were observed in any of the groups (Fig. 9). The implanted CaP paste was degraded to a large extent. More CaP paste remained in the CMC/CaP and CaP/PEI/pVEGF/SiO2 groups. In some places, CaP pastes were directly covered with bone or connective tissue. A few foreign body giant cells were observed around fragments. The bone defects were almost completely filled with new bone tissue in the 3mixCaP group. The immunohistological findings for TNF-α, OCN, Runx2, and SP-7 at 21 days after surgery are shown in Fig. 9. More TNF-α-positive cells were observed in the CaP/CMC, CaP/PEI/pVEGF/SiO_2, and CaP/PEI/pBMP-7/SiO_2 groups than in the 3mixCaP and CaP/PEI/siRNA-TNF-α/SiO_2 groups. An OCN-positive area was observed around the remaining CaP or the edge of bone cavity in all groups except CaP/PEI/pVEGF/SiO_2. Runx2-positive cells were observed around the remaining CaP in all groups. More SP7-positive cells were observed around the remaining CaP in the CaP/PEI/pBMP-7/SiO_2 groups and the CaP/PEI/siRNA-TNF-α/SiO_2 groups compared to the 3mixCaP, CaP/CMC, and CaP/PEI/pVEGF/SiO_2 groups. We previously demonstrated that BMP-2 which resulted from gene transfection induced by CaP loaded on implanted scaffolds was released at least until 28 days after implantation [29]. The successful gene transfection with CaP loading pBMP-7 or siRNA-TNF-α at 21 days after surgery will induce

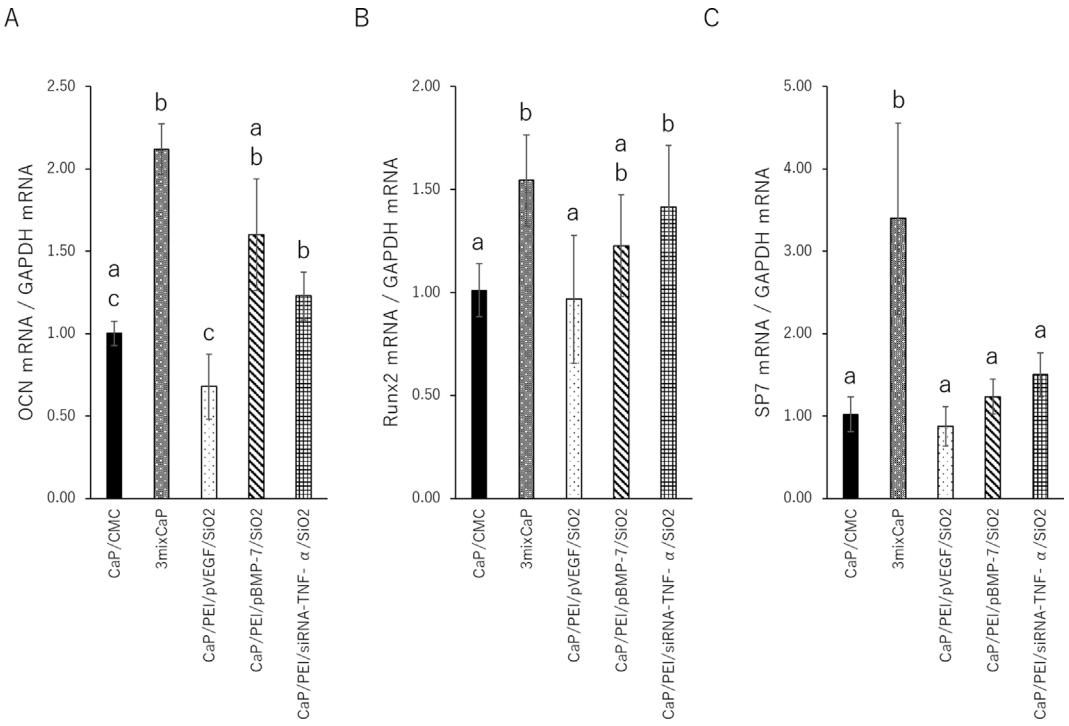

Fig. 7. Gene expression analyses. Concentrations of (A) OCN, (B) Runx2, and (C) SP-7 (Osterix) after 10 days of implantation in the femoral head. The values and error bars indicate the mean and standard deviation values, respectively. The number of samples in all groups was five. Significant differences ($p < 0.05$) between the groups at each time point are denoted by different superscript letters (i.e., bars with the same letter are not significantly different).

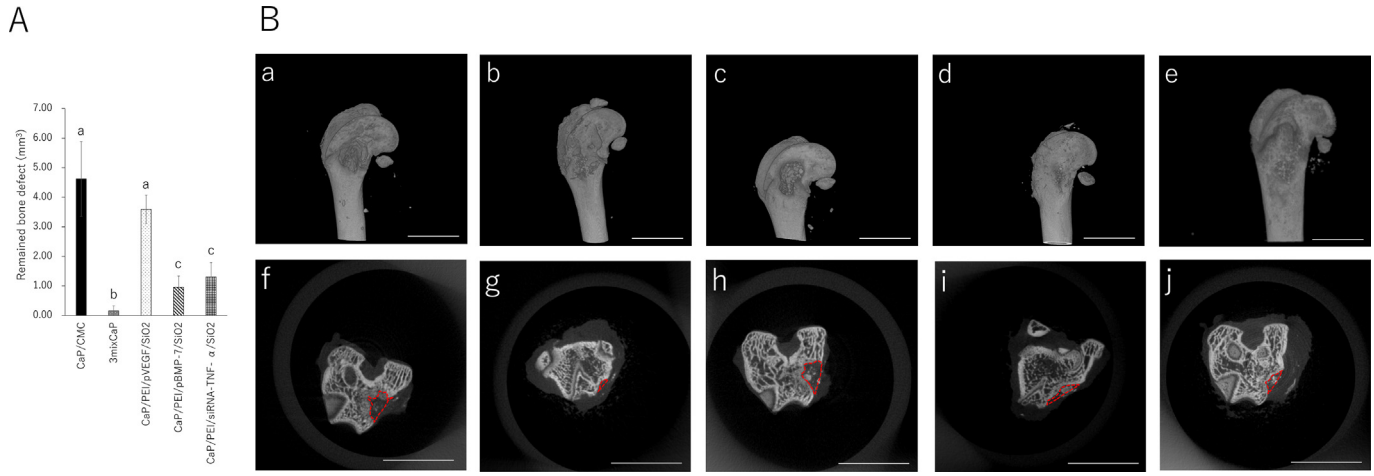

Fig. 8. (A) Remaining bone defect volume after 21 days of implantation in the femoral head. The values and error bars indicate the mean and standard deviation values, respectively. The number of samples in all groups was five. Significant differences ($p < 0.05$) between the groups at each time point are denoted by different superscript letters (i.e., bars with the same letter are not significantly different). (B) 3D μCT images of (a) CaP/CMC, (b) 3mixCaP, (c) CaP/PEI/pVEGF/SiO_2, (d) CaP/PEI/pBMP-7/SiO_2, and (e) CaP/PEI/siRNA-TNF-α/SiO_2. Cross-sectional μCT images at bone defect area of (f) CaP/CMC, (g) 3mixCaP, (h) CaP/PEI/pVEGF/SiO_2, (i) CaP/PEI/pBMP-7/SiO_2, and (j) CaP/PEI/siRNA-TNF-α/SiO_2 after 21 days of implantation in the femoral head. Scale bars in (a)–(e) are 5000 μm and those in (f)–(j) are 1 mm. The dotted line shows the outline of the remaining bone defect part.

the active bone formation in 3mixCaP, CaP/PEI/pBMP-7/SiO_2 and CaP/PEI/siRNA-TNF-α/SiO_2 as shown here.

CMC has a high biocompatibility and has been widely used for wound healing or tissue regeneration [32,33]; therefore, it was used as a base material in this study to coat the CaP nanoparticles. Based on histological observations, the CaP paste exhibited good biocompatibility and osteoconduction. Remnants of the CaP paste were found in all groups at 21 days after implantation. The remaining fragments were fewer in the 3mixCaP group, and foreign body giant cells were not observed around fragments. These observations are consistent with our previous report [31], in which a small fragment of CaP paste was observed without foreign body giant cells around CaP fragments after 4 weeks of implantation; however, most of the CaP pastes degraded after 12 weeks. The CaP nanoparticles used in this study had a core diameter of 100–200 nm. Small CaP particles are easily resorbed via internalization and intercellular digestion in endolysosomes [34]. Lin et al. reported that an increase in osteogenic activity, like by BMP-2 corporation, can mediate inflammation by restraining the participation of foreign body giant cells [35].

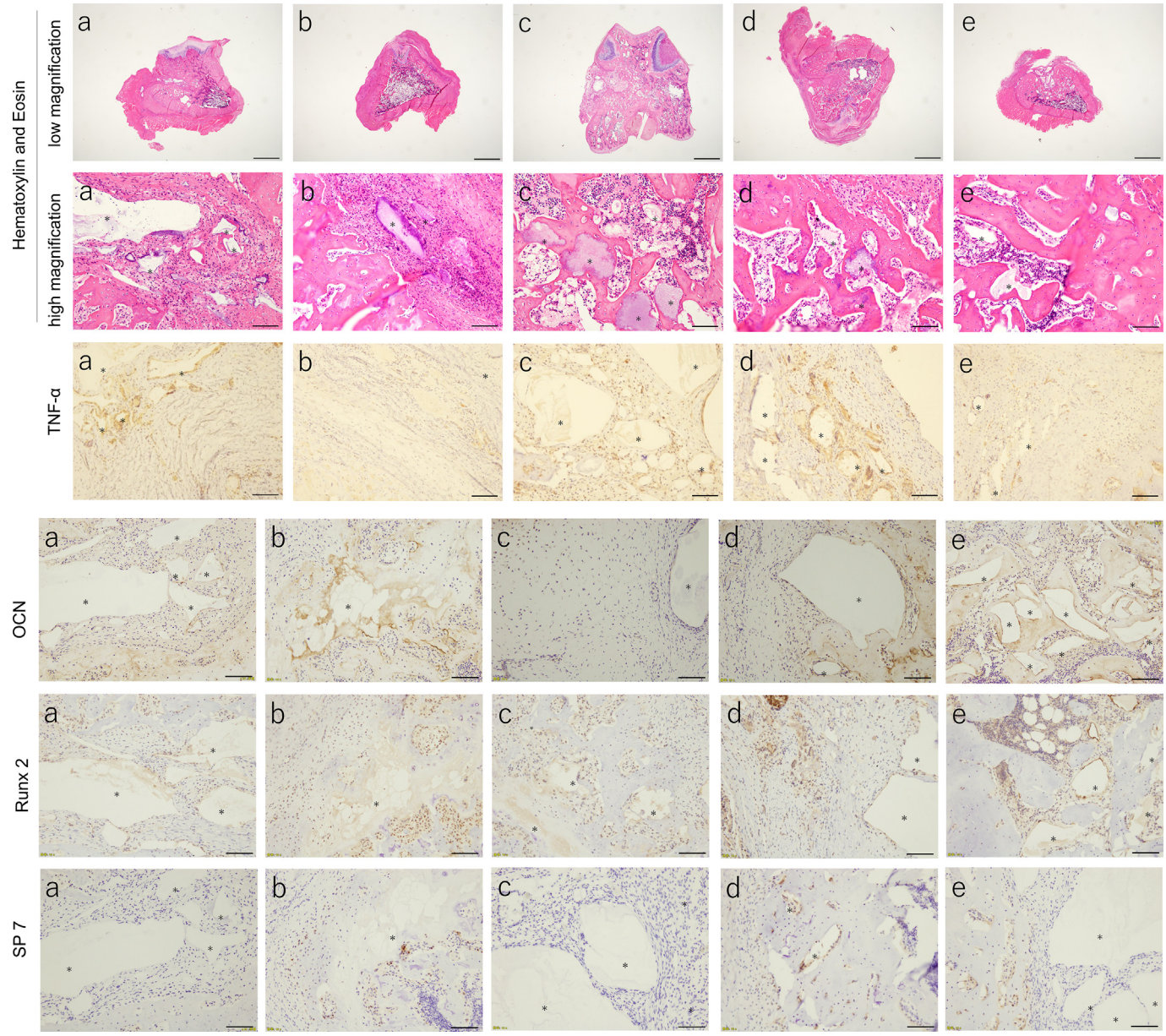

Fig. 9. Histological analysis after 21 days of implantation in the femoral head: (a) CaP/CMC, (b) 3mixCaP, (c) CaP/PEI/pVEGF/SiO_2, (d) CaP/PEI/pBMP-7/SiO_2, and (e) CaP/PEI/siRNA-TNF-α/SiO_2. The asterisk shows remaining implanted material (CaP). Scale bars: 1600 μm in low magnification of Hematoxylin and Eosin and 100 μm in high magnification of Hematoxylin and Eosin, TNF-α, OCN, Runx2 and SP-7.

The remaining bone defect volume of CaP/PEI/pBMP-7/SiO_2 21 days after surgery was smaller than that of CaP/CMC, and the ALP activity of CaP/PEI/pBMP-7/SiO_2 was higher in vitro. BMP-7 directly induces osteoblast differentiation [36]. This indicates that the released BMP-7 resulted from gene transfection and subsequently induced bone healing.

In contrast, the remaining bone defect volume of CaP/PEI/siRNA-TNF-α/SiO_2 was also smaller than that of CaP/CMC. TNF-α inhibits osteoblast differentiation [37,38]. Abbas et al. reported that TNF-α inhibits pre-osteoblast differentiation via core-binding factor A1 (cbfa1) activation [39]. The released volume of TNF-α decreased with the application of CaP/PEI/siRNA-TNF-α/SiO_2. The inhibition of the released TNF-α volume by gene silencing resulted in the enhancement of bone healing in this study. Interestingly, the remaining bone defect volume in CaP/PEI/siRNA-TNF-α/SiO_2 was comparable to that in CaP/PEI/pBMP-7/SiO_2. This suggests that the inhibition of TNF-α is a useful therapy for bone regeneration or repair, in addition to the conventional treatment in which bone formation-related growth factors are applied. Regarding the safety of siRNA, numerous gene therapies using siRNA have been developed for mRNA targeting, and they are in the clinical trial stage of investigation. Gene therapy using siRNA has been approved by the Food and Drug Administration (FDA) in the USA [40].

The inhibition of VEGF activity disrupts the repair of femoral fractures and cortical bone defects [41]; therefore, VEGF activity is essential for angiogenesis and bone healing.

CD31 is a marker of vascular endothelial cells. CD31 in CaP/PEI/pVEGF/SiO_2 and 3mixCaP was higher than that in CaP/CMC, CaP/PEI/pBMP-7/SiO_2, and CaP/PEI/siRNA-TNF-α/SiO_2 (Fig. 5D). This indicates that vascularization by VEGF release resulting from gene transfection might succeed. VEGF promotes angiogenesis, induces bone-formation-related growth factors, recruits bone-formation-

related cells, and induces the differentiation of osteoblasts and indirectivity to form new bone tissue [1,2]. However, in the present study, the remaining bone defect volume of CaP/PEI/pVEGF/SiO_2 was comparable to that of CaP/CMC. Some studies demonstrated that bone formation was not improved or enhanced in a bone defect model by the single application of VEGF, while the values of VEGF expression, cell numbers, blood vessel area, and blood vessel volume were high [42–46]. On the other hand, the amounts of BMP-2 and BMP-7 in 3mix/CaP were higher than those in CaP/PEI/pVEGF/SiO_2, and the concentration of CD31 was approximately the same in this study. This indicates that the management of the microenvironment after vascularization might be important for bone tissue regeneration.

In this study, bone healing was most enhanced in the case of 3mixCaP. The concentrations of BMP2, VEGF, and TNF-α were significantly different from that of CaP/CMC, and the expressions of OCN, Runx2, and SP7 both at protein and gene levels were the highest in all groups. This indicates that the (simultaneous) release of different growth factors together with the reduction of inflammatory cytokines independently contributed to bone formation in the 3mixCaP group. First, BMP-7 itself exhibits strong osteogenesis [36]. Second, TNF-α inhibits BMP-induced osteoblast differentiation by activating SAPK/JNK signaling [47]. The inhibition of TNF-α release by gene silencing not only removes suppression and inhibits osteoblastogenesis by TNF-α but also enhance BMP-induced bone formation. Ratanavaraporn et al. demonstrated a significant inhibition of TNF-α-enhanced bone regeneration following BMP-2 application [17]. BMP enhances bone formation via several signaling pathways [48–50]. BMP-7 induces bone formation via the SMAD pathway [51]; thus, bone formation through the inhibition of TNF-α might have occurred independently via a different pathway in this study. Third, the vascularization resulting from VEGF release might recruit much more osteogenesis-associated cells or growth factors like BMP-2 by local stimulation of osteogenesis-associated growth factors like BMP-7. The release amounts of BMP-2 or BMP-7 in 3mixCaP was higher in this study.

In general, viral vectors have a higher gene transfection efficiency than nonviral vectors; however, the risk of cytotoxicity [52], immunogenicity [53], and potential recombination or complementation [54] cannot be neglected for viral vectors. Cell activities like proliferation, differentiation, or intercell interactions are high in tissue regeneration or repair reactions. Avoiding these risks is advantageous for tissue regeneration therapy. By contrast, plasmid DNA generally does not transfect by itself and is degraded in cells and tissue by nucleases; thus, a nonviral gene delivery was used in this study, i.e. a nanoparticle with encapsulated nucleic acids. A nonviral transfection is therefore transient in nature and not permanent. In addition, the presence of calcium phosphate will induce bone formation by itself [21].

The present study demonstrated the usefulness of a simultaneous BMP-7 and VEGF release and TNF-α inhibition for bone regeneration. However, the applied doses of plasmid-DNA or siRNA were not varied in this study as this would have required hundreds of test animals. Furthermore, the bone defects prepared in this study were not of a critical size. In the future, the relationship between the adequate dose of plasmid-DNA or siRNA and the bone defect size should be assessed for bone tissue regeneration.

4. Conclusion

In this comprehensive animal study, we evaluated bone healing in bone defects prepared in the rat femoral head by gene transfection and gene silencing techniques with DNA- and siRNA-loaded CaP nanoparticles, applied as a paste. The application of the DNA-loaded CaP nanoparticle paste induced a successful local biosynthesis of BMP-7 and VEGF, respectively, and the application of a siRNA-loaded CaP nanoparticle paste successfully inhibited the biosynthesis of TNF-α. The CaP paste, including either plasmid DNA encoding for BMP-7 or siRNA inhibiting TNF-α, significantly enhanced bone healing after 3 weeks of implantation compared to the case of a CaP control paste without nucleic acids. OCN, Runx2, and SP7 were significantly increased at the protein and gene levels in a CaP paste containing both types of DNA (BMP-7 and VEGF-A) as well as siRNA inhibiting TNF-α, 10 days after implantation. This triple-functionalized CaP paste most significantly accelerated bone healing. In summary, the triple-functionalized CaP paste containing plasmid DNA encoding for BMP-7 or VEGF and siRNA inhibiting TNF-α is a promising gene therapeutic for enhanced bone regeneration, e.g. in orthopedic surgery and dental surgery.

Declaration of Generative AI and AI-assisted technologies in the writing process

The authors state that we did not use any generative artificial intelligence (AI) and AI-assisted technologies in the writing process.

Declaration of competing interest

The authors declare that they have no known competing financial interests or personal relationships that could have appeared to influence the work reported in this paper.

Acknowledgments

This study was financially supported by a Grant-in-Aid for Scientific Research from the Japan Society for the Promotion of Science (JPJSBP120203501 and JPJSBP120233502) in Japan and the Deutscher Akademischer Austauschdienst (DAAD). The funders played no role in the design, decision to publish, preparation of the manuscript, or data collection and analysis.

References

[1] Martino MM, Briquez PS, Maruyama K, Hubbell JA. Extracellular matrix-inspired growth factor delivery systems for bone regeneration. Adv Drug Deliv Rev 2015;94:41–52.
[2] Stegen S, van Gastel N, Carmeliet G. Bringing new life to damaged bone: the importance of angiogenesis in bone repair and regeneration. Bone 2015;70:19–27.
[3] Kempen DH, Creemers LB, Alblas J, Lu L, Verbout AJ, Yaszemski MJ, Dhert WJ. Growth factor interactions in bone regeneration, Tissue Eng. Part B Rev 2010;6:551–66.
[4] Gothard D, Smith EL, Kanczler JM, Rashidi H, Qutachi O, Henstock J, Rotherham M, El Haj A, Shakesheff KM, Oreffo RO. Tissue engineered bone using select growth factors: a comprehensive review of animal studies and clinical translation studies in man. Eur Cell Mater 2014;28:166–208.
[5] Hughes FJ, Turner W, Belibasakis G, Martuscelli G. Effects of growth factors and cytokines on osteoblast differentiation. Periodontol 2000 2006;41:48–72.
[6] Axelrad TW, Einhorn TA. Bone morphogenetic proteins in orthopaedic surgery. Cytokine Growth Factor Rev 2009;5–6:481–8.
[7] Cheline AJ, Reddi AH, Martin RB. Bone morphogenetic protein-7 selectively enhances mechanically induced bone formation. Bone 2002;5:570–4.
[8] Chen TL, Shen WJ, Kraemer FB. Human BMP-7/OP-1 induces the growth and differentiation of adipocytes and osteoblasts in bone marrow stromal cell cultures. J Cell Biochem 2001;82:187–99.
[9] Mantripragada VP, Jayasuriya AC. Bone regeneration using injectable BMP-7 loaded chitosan microparticles in rat femoral defect. Mater Sci Eng C 2016;63:596–608.
[10] Hirschi KK, Skalak TC, Peirce SM, Little CD. Vascular assembly in natural and engineered tissues. AnnNY Acad Sci 2002;961:223.
[11] Ribatti D. The crucial role of vascular permeability factor/vascular endothelial growth factor in angiogenesis: a historical review. Br J Haematol 2005;128:303.
[12] Hu K, Olsen BR. The roles of vascular endothelial growth factor in bone repair and regeneration. Bone 2016;91:30–8.
[13] Peng H, Usas A, Olshanski A, Ho AM, Gearhart B, Cooper GM, Huard J. VEGF improves, whereas sFlt1 inhibits, BMP2-induced bone formation and bone

healing through modulation of angiogenesis. J Bone Miner Res 2005;20:2017–27.
[14] Bek S, Nielsen JV, Bojesen AB, Franke A, Bank S, Vogel U, Andersen V. Systematic review: genetic biomarkers associated with anti-TNF treatment response in inflammatory bowel diseases. Aliment Pharmacol Ther 2016;44:554–67.
[15] Pacios S, Kang J, Galicia J, Gluck K, Patel H, Ovaydi-Mandel A, Petrov S, Alawi F, Graves DT. Diabetes aggravates periodontitis by limiting repair through enhanced inflammation. Faseb J 2012;26:1423–30.
[16] Cirelli JA, Park CH, MacKool K, Taba M, Lustig KH, Burstein H, Giannobile WV. AAV2/1-TNFR:Fc gene delivery prevents periodontal disease progression. Gene Ther 2009;16:426–36.
[17] Ratanavaraporn J, Furuya H, Tabata Y. Local suppression of pro-inflammatory cytokines and the effects in BMP-2-induced bone regeneration. Biomaterials 2012;33:304–16.
[18] Tenkumo T, Rojas-Sánchez L, Vanegas Sáenz JR, Ogawa T, Miyashita M, Yoda N, Prymak O, Sokolova V, Sasaki K, Epple M. Reduction of inflammation in a chronic periodontitis model in rats by TNF-α gene silencing with a topically applied siRNA-loaded calcium phosphate paste. Acta Biomater 2020;105:263–79.
[19] Wegman F, Oner FC, Dhert WJ, Alblas J. Non-viral gene therapy for bone tissue engineering. Biotechnol Genet Eng Rev 2013;29:206–20.
[20] Shapiro G, Lieber R, Gazit D, Pelled G. Recent advances and future of gene therapy for bone regeneration. Curr Osteoporos Rep 2018;16:504–11.
[21] Sokolova V, Epple M. Biological and medical applications of calcium phosphate nanoparticles. Chem Eur J 2021;27:7471–88.
[22] Hadjicharalambous C, Kozlova D, Sokolova V, Epple M, Chatzinikolaidou M. Calcium phosphate nanoparticles carrying BMP-7 plasmid DNA induce an osteogenic response in MC3T3-E1 pre-osteoblasts. J Biomed Mater Res A 2015;103:3834–42.
[23] Kozlova D, Chernousova S, Knuschke T, Buer J, Westendorf AM, Epple M. Cell targeting by antibody-functionalized calcium phosphate nanoparticles. J Mater Chem 2012;22:396–404.
[24] Sokolova VV, Radtke I, Heumann R, Epple M. Effective transfection of cells with multi-shell calcium phosphate-DNA nanoparticles. Biomaterials 2006;27:3147–53.
[25] Epple M, Ganesan K, Heumann R, Klesing J, Kovtun A, Neumann S, et al. Application of calcium phosphate nanoparticles in biomedicine. J Mater Chem 2010;20:18–23.
[26] Sokolova V, Neumann S, Kovtun A, Chernousova S, Heumann R, Epple MA. Outer shell of positively charged poly(ethyleneimine) strongly increases the transfection efficiency of calcium phosphate-DNA nanoparticles. J Mater Sci 2010;45:4952–7.
[27] Xiang C, Tenkumo T, Ogawa T, Kanda Y, Nakamura K, Shirato M, Sokolova V, Epple M, Kamano Y, Egusa H, Sasaki K. Gene transfection achieved by utilizing antibacterial calcium phosphate nanoparticles for enhanced regenerative therapy. Acta Biomater 2021;119:375–89.
[28] Klesing J, Chernousova S, Epple M. Freeze-dried cationic calcium phosphate nanorods as versatile carriers of nucleic acids (DNA, siRNA). J Mater Chem 2012;22:199–204.
[29] Tenkumo T, Vanegas Sáenz JR, Nakamura K, Shimizu Y, Sokolova V, Epple M, Kamano Y, Egusa H, Sugaya T, Sasaki K. Prolonged release of bone morphogenetic protein-2 in vivo by gene transfection with DNA-functionalized calcium phosphate nanoparticle-loaded collagen scaffolds. Mater Sci Eng C 2018;92:172–83.
[30] Chernousova S, Klesing J, Soklakova N, Epple M. A genetically active nano-calcium phosphate paste for bone substitution, encoding the formation of BMP-7 and VEGF-A. RSC Adv 2013;3:11155–61.
[31] Schlickewei C, Klatte TO, Wildermuth Y, Laaff G, Rueger JM, Ruesing J, Chernousova S, Lehmann W, Epple M. A bioactive nano-calcium phosphate paste for in-situ transfection of BMP-7 and VEGF-A in a rabbit critical-size bone defect: results of an in vivo study. J Mater Sci Mater Med 2019;30:15.
[32] Kanikireddy V, Varaprasad K, Jayaramudu T, Karthikeyan C, Sadiku R. Carboxymethyl cellulose-based materials for infection control and wound healing: a review. Int J Biol Macromol 2020;164:963–75.
[33] Qi P, Ohba S, Hara Y, Fuke M, Ogawa T, Ohta S, Ito T. Fabrication of calcium phosphate-loaded carboxymethyl cellulose non-woven sheets for bone regeneration. Carbohydr Polym 2018;189:322–30.
[34] Stastny P, Sedlacek R, Suchy T, Lukasova V, Rampichova M, Trunec M. Structure degradation and strength changes of sintered calcium phosphate bone scaffolds with different phase structures during simulated biodegradation in vitro. Mater Sci Eng C 2019;100:544–53.
[35] Lin X, de Groot K, Wang D, Hu Q, Wismeijer D, Liu Y. A review paper on biomimetic calcium phosphate coatings. Open Biomed Eng J 2015;9:56–64.
[36] Hankenson KD, Gagne K, Shaughnessy M. Extracellular signaling molecules to promote fracture healing and bone regeneration. Adv Drug Deliv Rev 2015;94:3–12.
[37] Gilbert L, He X, Farmer P, Boden S, Kozlowski M, Rubin J, Nanes MS. Inhibition of osteoblast differentiation by tumor necrosis factor-α. Endocrinology 2000;141:3956–64.
[38] Gilbert L, He X, Farmer P, Rubin J, Drissi H, van Wijnen AJ, Lian JB, Stein GS, Nanes MS. Expression of the osteoblast differentiation factor RUNX2 (Cbfa1/AML3/Pebp2αA) is inhibited by tumor necrosis factor-α. J Biol Chem 2002;277:2695–701.
[39] Abbas S, Zhang YH, Clohisy JC, Abu-Amer Y. Tumor necrosis factor-alpha inhibits pre-osteoblast differentiation through its type-1 receptor. Cytokine 2003;22:33–41.
[40] Dong Y, Siegwart DJ, Anderson DG. Strategies, design, and chemistry in siRNA delivery systems. Adv Drug Deliv Rev 2019;144:133–47.
[41] Street J, Bao M, de Guzman L, Bunting S, Peale FV, Jr Ferrara N, Steinmetz H, Hoeffel J, Cleland JL, Daugherty A, van Bruggen N, Redmond HP, Carano RA, Filvaroff EH. Vascular endothelial growth factor stimulates bone repair by promoting angiogenesis and bone turnover. Proc Natl Acad Sci USA 2002;99:9656.
[42] Zhang W, Zhu C, Wu Y, Ye D, Wang S, Zou D, Zhang X, Kaplan DL, Jiang X. VEGF and BMP-2 promote bone regeneration by facilitating bone marrow stem cell homing and differentiation. Eur Cell Mater 2014;27:1–12.
[43] Patel ZS, Young S, Tabata Y, Jansen JA, Wong ME, Mikos AG. Dual delivery of an angiogenic and an osteogenic growth factor for bone regeneration in a critical size defect model. Bone 2008;43:931–40.
[44] Kempen DH, Lu L, Heijink A, Hefferan TE, Creemers LB, Maran A, Yaszemski MJ, Dhert WJ. Effect of local sequential VEGF and BMP-2 delivery on ectopic and orthotopic bone regeneration. Biomaterials 2009;30:2816–25.
[45] Samee M, Kasugai S, Kondo H, Ohya K, Shimokawa H, Kuroda S. Bone morphogenetic protein-2 (BMP-2) and vascular endothelial growth factor (VEGF) transfection to human periosteal cells enhances osteoblast differentiation and bone formation. J Pharmacol Sci 2008;108:18–31.
[46] Zhang W, Wang X, Wang S, Zhao J, Xu L, Zhu C, Zeng D, Chen J, Zhang Z, Kaplan DL, Jiang X. The use of injectable sonication-induced silk hydrogel for VEGF(165) and BMP-2 delivery for elevation of the maxillary sinus floor. Biomaterials 2011;32:9415–24.
[47] Mukai T, Otsuka F, Otani H, Yamashita M, Takasugi K, Inagaki K, Yamamura M, Hakino. TNF-alpha inhibits BMP-induced osteoblast differentiation through activating SAPK/JNK signaling. Biochem Biophys Res Commun 2007;356:1004–10.
[48] Canalis E, Economides AN, Gazzerro E. Bone morphogenetic proteins, their antagonists, and the skeleton. Endocr Rev 2003;24:218–35.
[49] Wu M, Chen G, Li YP. TGF-β and BMP signaling in osteoblast, skeletal development, and bone formation, homeostasis and disease. Bone Res 2016;26:16009.
[50] Lowery JW, Rosen V. The BMP pathway and its inhibitors in the skeleton. Physiol Rev 2018;98:2431–52.
[51] Saini S, Duraisamy AJ, Bayen S, Vats P, Singh SB. Role of BMP7 in appetite regulation, adipogenesis, and energy expenditure. Endocrine 2015;48:405–9.
[52] Herz J, Gerard RD. Adenovirus mediated transfer of low density lipoprotein receptor gene acutely accelerates cholesterol clearance in normal mice. Proc Natl Acad Sci USA 1993;90:2812–6.
[53] Simon RH, Engelhardt JF, Yang Y, Zepeda M, Weber-Pendleton S, Grossman M, et al. Adenovirus mediated transfer of the CFTR gene to lung of nonhuman primates: toxicity study. Hum Gene Ther 1993;4:771–80.
[54] Walther W, Stein U. Viral vectors for gene transfer: a review of their use in the treatment of human diseases. Drugs 2000;60:249–71.